Linearized Transport Model for Nanofiltration: Development and Assessment

W. Richard Bowen, Julian S. Welfoot, and Paul M. Williams
Centre for Complex Fluids Processing, Dept. of Chemical and Biological Process Engineering, University of Wales Swansea, Singleton Park, Swansea, SA2 8PP, UK

Finite difference linearization of pore concentration gradient in nanofiltration membranes greatly simplifies the solution of a three-parameter model (pore radius, membrane charge, and pore dielectric constant) for electrolyte rejection by removing the requirement for numerical integration of the extended Nernst–Planck equation. The validity of the linearized model is first experimentally tested by comparing with a rigorous characterization of the Desal-DK nanofiltration membrane, the linearized model closely agreeing with the numerical solution of the full model. Investigation of pore concentration profiles showed the assumption of linearity to be valid over a wide range of nanofiltration conditions. The linearized model was also successfully extended to ternary electrolyte mixtures, highlighting its main advantage over analytic solutions. Overall, the model is a powerful tool for characterization of nanofiltration membranes and subsequent prediction of separation performance. Computational demands are modest in terms of time and complexity.

Introduction

Nanofiltration (NF) is the most recently developed pressure-driven membrane process for liquid-phase separations. The properties of NF membranes (where pores are nominally ~1 nm in dimension) lie between those of nonporous reverse-osmosis (RO) membranes and porous ultrafiltration (UF) membranes, solutes being separated by a combination of size, electrical, and dielectric mechanisms. NF membranes have been found to be extremely effective in the fractionation and selective removal of solutes from complex process streams. This development of NF technology as a viable process during the last decade has led to a marked increase in its adoption in a number of industries, such as treatment of pulp-bleaching effluents from the textile industry (Rosa and de Pinho, 1995), separation of pharmaceuticals from fermentation broths (Tsuru et al., 1994), demineralization in the dairy industry (van der Horst et al., 1995), metal recovery from wastewater (Fane et al., 1992), and virus removal (Hoffer et al. 1995).

Almost all existing predictive models of NF separations employ an equilibrium partitioning expression to describe the distribution of ions at the pore inlet and outlet, with pore transport being described by the extended Nernst–Planck equation (Tsuru et al., 1991a; Wang et al., 1997; Combe et al., 1997; Bowen and Mohammad, 1998; Afonso and de Pinho, 2000). These models describe electrolyte rejection at a given volume flux, J_v, in terms of three parameters (effective pore radius, r_p, effective ratio of membrane thickness to porosity, $\Delta x/A_k$, and effective membrane charge density, X_d). Solution of the governing equations in these models requires nonlinear numerical methods because exact integral solutions of transport equations are extremely complex and do not readily yield quantitative explicit evaluation of permeate concentrations (Schlögl, 1966). This notwithstanding, Tsuru et al. (1991a) derived such an analytical solution for univalent electrolytes using a purely Donnan partitioning expression to define permeate concentration in terms of normalized flux ($J_v\Delta x/A_k$) and membrane charge density. However, this approach could not be extended to more complex systems, and so Runge–Kutta numerical integration was still performed in predictions of the rejection of other electrolytes.

Weaknesses of such existing models lie in the extremely large predicted values of X_d (Bowen and Mohammad, 1998) and the use of $\Delta x/A_k$ as a fitting parameter to obtain good agreement with experimental rejection data. This empirical nature of such NF modeling has limited the success of predictions of more complex systems due to difficulties in predicting X_d (from the adsorption isotherms of single elec-

Correspondence concerning this article should be addressed to W. R. Bowen.

trolytes), as this parameter dominates the model in many cases.

The application of NF in industrial separations also has highlighted the limitations of existing predictive models in terms of process design. The current trend in modeling is to develop physical realism in order to improve the agreement between model parameters and measured physical properties. This can lead to models of great complexity that are difficult to apply in practice. Conversely, no reliable general model has been yet developed for approximate prediction of NF performance that can be adopted by nonspecialist engineers in the preliminary assessment of a given separation.

The preceding NF descriptions encompass a number of separation mechanisms that are each capable of dominating overall transport, under certain conditions. Therefore, it is not straightforward to simplify existing models for the general case because all mechanisms must be retained. Schlögl (1966) discussed the linearization of transport in homogeneous membrane phases and stated that the linearization of potential gradient is, in general, much more appropriate than concentration gradient due to nonlinearities in pore concentration profiles at increased volume fluxes. The proposed model was not, however, tested experimentally.

Dresner (1972) dismissed such an approximation of potential gradient for most hyperfiltration (RO) conditions, and instead proposed a simplification for prediction of asymptotic rejection at membranes with almost complete exclusion of coions. The diffusion component was neglected from transport, as pore concentrations were assumed to be independent of position almost immediately downstream of the pore inlet. Again, no experimental verification of this assumption was provided. Van der Horst et al. (1995) linearized both concentration and potential gradient in their study of ternary salt mixtures, but no equilibrium partitioning expression was included and transport parameters were obtained that gave no information on membrane structure or electrical properties. Sarrade et al. (1994) also neglected diffusive transport in their study of inorganic NF membranes, and Rios et al. (1996) were able to successfully develop their approach to describe the rejection of both single and multicomponent electrolytes.

In the present article, a simplified approach is proposed that is based upon a model for uncharged solute rejection with one independent parameter (pore radius) and a model for electrolyte rejection with three independent parameters (pore radius, membrane charge, and pore dielectric constant) (all other variables being calculated on a defined basis). The introduction of dielectric exclusion in this model significantly reduces the magnitude of predicted values of X_d and changes the emphasis from X_d to pore radius (through pore dielectric constant) as the dominant parameter. Finite difference linearization of pore concentration gradients reduces the system of first-order differential transport equations to a system of algebraic equations, removing the requirement for numerical integration. This linearized model is applied to the characterization of a widely used NF membrane (Desal-DK), and the validity of the approach is investigated over a wide range of NF operating conditions. The advantage of the linearization approach over analytical solutions is highlighted when the calculations are extended to the separation of univalent-divalent ternary-ion mixtures. Comparison is made throughout to the results obtained with the full equations.

Theoretical Aspects

Rejection of single electrolytes

Statement of the Full Problem. The overall solution of models based on the extended Nernst–Planck equation [the extended Nernst–Planck equation is a simple version of the Stefan–Maxwell approach (Wesselingh and Krishna, 2000); a full implementation of the Stefan–Maxwell approach is not possible for the present problem due to lack of data (Bowen and Mohammad, 1998) is an iterative calculation because of the presence of permeate concentrations in the derived transport equations, even when an analytical solution of pore transport has been derived for a simple case. In the present article, the extended Nernst–Planck equation describes pore-ion transport

$$j_i = -D_{i,p}\frac{dc_i}{dx} - \frac{z_i c_i D_{i,p}}{RT}F\frac{d\psi}{dx} + K_{i,c}c_i V \tag{1}$$

It is usual, through use of the conditions of pore electroneutrality and zero current, to use Eq. 1 to obtain an expression for potential gradient

$$\frac{d\psi}{dx} = \frac{\frac{z_1 V}{D_{1,p}}\left(K_{1,c}c_i - C_{1,p}\right) + \frac{z_2 V}{D_{2,p}}\left(K_{2,c}c_2 - C_{2,p}\right)}{\frac{F}{RT}\left(z_1^2 c_1 + z_2^2 c_2\right)} \tag{2}$$

The concentrations of ion 2, c_2, and $C_{2,p}$, can be eliminated from Eq. 2 using the electroneutrality conditions within the pore and the permeate solutions. By definition

$$z_1 c_1 + z_2 c_2 + X_d = 0 \qquad \therefore c_2 = \frac{z_1 c_1 + X_d}{-z_2} \tag{3}$$

$$z_1 C_{1,p} + z_2 C_{2,p} = 0 \qquad \therefore C_{2,p} = -\frac{z_1}{z_2}C_{1,p} \tag{4}$$

Substitution of Eqs. 3 and 4 into Eq. 2 and rearrangement yields

$$\frac{F}{RT}\frac{d\psi}{dx} = \frac{z_1 V\left(\frac{K_{1,c}}{D_{1,p}} - \frac{K_{2,c}}{D_{2,p}}\right)c_1 - z_1 V\left(\frac{1}{D_{1,p}} - \frac{1}{D_{2,p}}\right)C_{1,p} - \frac{K_{2,c}V}{D_{2,p}}X_d}{\left(z_1^2 - z_1 z_2\right)c_1 - z_2 X_d} \tag{5}$$

The concentration gradient for ion 1 is related to potential gradient as follows

$$\frac{dc_1}{dx} = \frac{V}{D_{1,p}}\left(K_{1,c}c_1 - C_{1,p}\right) - z_1\frac{F}{RT}c_1\frac{d\psi}{dx} \tag{6}$$

There is, of course, a corresponding expression for ion 2, but this will be dependent of Eq. 6 because of pore electroneutrality. The equilibrium partitioning of ions at the pore inlet and outlet in this model will be assumed to result from a combination of steric effects (due to the finite sizes of the ions and the pore), electrical effects (defined through the

Donnan potential), and dielectric exclusion (where an energy barrier to solvation is developed by a reduction of pore dielectric constant within the pore)

$$\frac{c_i}{C_i} = \Phi_i \exp\left(\frac{-z_i F}{RT}\Delta\psi_D\right)\exp\left(\frac{-\Delta W_i}{kT}\right) \tag{7}$$

The solvation energy barrier is defined through the Born model (Born, 1920)

$$\Delta W_i = \frac{z_i^2 e^2}{8\pi\epsilon_0 a_i}\left(\frac{1}{\epsilon_p} - \frac{1}{\epsilon_b}\right) \tag{8}$$

This expression is sufficient if the pores are assumed to be of uniform radius, since it is does not require knowledge of the solvent structure within the pores. However, a significant distribution of pore radii would make it necessary to relate average pore dielectric constant to pore radius (as will be discussed in the subsection titled "Range of Validity of Linearized Concentration Gradients").

The system of equations defined here (Eqs. 5, 6, 7, and 8) will be termed the full model for electrolyte rejection throughout the present article. The normal solution method involves the adoption of a fourth-order Runge–Kutta algorithm in the simultaneous stepwise integration of the concentration and potential gradients (Dresner, 1972). However, it is possible, through finite difference (FD) linearization of the concentration gradient, to remove the requirement for numerical integration.

Rejection of 1:1 Electrolytes Using Linearization. Many characterization studies employ uni-univalent electrolytes such as NaCl, and so these will be used here to demonstrate the method applied for all single electrolytes. In this case $C_{1,w} = C_{2,w} = C_w$, $C_{1,p} = C_{2,p} = C_p$, $z_1 = -z_2 = 1$, and so Eq. 5 becomes

$$\frac{F}{RT}\frac{d\psi}{dx} = \frac{\left(\frac{K_{1,c}V}{D_{1,p}} - \frac{K_{2,c}V}{D_{2,p}}\right)c_1 - \left(\frac{V}{D_{1,p}} - \frac{V}{D_{2,p}}\right)C_p - \left(\frac{K_{2,c}V}{D_{2,p}}\right)X_d}{2c_1 + X_d} \tag{9}$$

Substitution of Eq. 9 into Eq. 6 and rearrangement yields

$$\frac{dc_1}{dx} = \frac{\left(\frac{K_{1,c}V}{D_{1,p}} + \frac{K_{2,c}V}{D_{2,p}}\right)c_1^2 + \left[\left(\frac{K_{1,c}V}{D_{1,p}} + \frac{K_{2,c}V}{D_{2,p}}\right)X_d - \left(\frac{V}{D_{1,p}} + \frac{V}{D_{2,p}}\right)C_p\right]c_1 - \frac{V}{D_{1,p}}X_d C_p}{2c_1 + X_d} \tag{10}$$

Inspection of Eq. 10 indicates that the order of the numerator is one higher than the denominator. The concentration gradient will be effectively constant (and hence the concentration profiles linear) provided the effect of the c^2 term is relatively small. Under these conditions, the concentration gradient can be approximated as follows

$$\frac{\Delta c_1}{\Delta x} = \frac{\left(\frac{K_{1,c}V}{D_{1,p}} + \frac{K_{2,c}V}{D_{2,p}}\right)c_{1,\mathrm{av}}^2 + \left[\left(\frac{K_{1,c}V}{D_{1,p}} + \frac{K_{2,c}V}{D_{2,p}}\right)X_d - \left(\frac{V}{D_{1,p}} + \frac{V}{D_{2,p}}\right)C_p\right]c_{1,\mathrm{av}} - \frac{V}{D_{1,p}}X_d C_p}{2c_{1,\mathrm{av}} + X_d} \tag{11}$$

where

$$\frac{dc_1}{dx} \approx \frac{\Delta c_1}{\Delta x} = \frac{c_1(\Delta x) - c_1(0)}{\Delta x} \quad \text{and} \quad c_{1,\mathrm{av}} = \frac{c_1(0) + c_1(\Delta x)}{2} \tag{12}$$

This expression can be greatly simplified by the introduction of the dimensionless Peclet number for each ion. Inclusion of the Hagen–Poiseuille definition of pore solvent velocity allows the Peclet number to be defined in terms of effective pressure ΔP_e

$$Pe_i = \frac{K_{i,c}V\Delta x}{D_{i,p}} = \frac{K_{i,c}\Delta x}{D_{i,p}}\left(\frac{r_p^2\Delta P_e}{8\eta\Delta x}\right) = \frac{K_{i,c}r_p^2\Delta P_e}{8D_{i,p}\eta} \tag{13}$$

Bowen and Mohammad (1998) successfully applied such a Hagen–Poiseuille relationship to predict volumetric flux, J_v, during dye-salt diafiltration with the CA30 NF membrane. The definition of ΔP_e in the present article differs from that based on irreversible thermodynamics where an osmotic (Staverman) reflection coefficient is included to account for the transport of solutes across the membrane. In the present case, $\Delta\pi$ is calculated on a dynamic basis that directly takes pore inlet and outlet concentrations (through C_w and C_p, respectively) into account (Bowen and Mohammad, 1998). The validity of the present approach was investigated using the experimental rejection of NaCl as a function of concentration (where R covered almost the entire possible range of rejection). A plot of J_v vs. ΔP_e showed very good linearity over the entire experimental range of ΔP_e and salt concentration, providing experimental justification for such a definition of ΔP_e. Furthermore, the linearity of such a plot indicated that electrokinetic effects (that could have been most conveniently introduced as an electroviscous term) were not significant. This is also expected theoretically (Bowen and Jenner, 1995), as in the present case the pores are sufficiently narrow, the membrane charge sufficiently small, and pore counterion concentrations sufficiently low (due to the introduction of dielectric exclusion) to prevent development of elec-

trical double layers in the NF pores. This is consistent with the assumption of radial potential and concentration homogeneity in many existing NF models (Wang et al., 1997; Bowen et al., 1997). It should be noted that the relative insignificance of electroviscous effects in nanofiltration is in contrast to their potential importance in ultrafiltration (Saksena and Zydney, 1995).

This notwithstanding, the pore viscosity in Eq. 13 will differ from the bulk viscosity because of increased solvent structure within the pore due to confinement. The earlier definition of Peclet number, and hence rejection, would be independent of viscosity if the pore diffusion coefficient was linearly scaled by an increase in viscosity, as the effects would cancel. A variation of pore viscosity with pore radius would, however, be extremely important in the analysis of pore-size distributions where overall rejection is dependent on the proportion of the total flux going through each class of pore. Inclusion of Eq. 13 in Eq. 11 and rearrangement yields the following explicit expression for C_p

$$C_p = \frac{(Pe_1 + Pe_2)c_{1,\mathrm{av}}^2 + (Pe_1 + Pe_2)X_d c_{1,\mathrm{av}} - (2c_{1,\mathrm{av}} + X_d)\Delta c_1}{\left(\frac{Pe_1}{K_{1,c}} + \frac{Pe_2}{K_{2,c}}\right)c_{1,\mathrm{av}} + \frac{Pe_1}{K_{1,c}}X_d} \tag{14}$$

This expression, in conjunction with Eq. 13, indicates that permeate concentration (and hence rejection) is also independent of membrane thickness. Previous theoretical analyses and fitting procedures that considered rejection as a function of volumetric flux (J_v) have allowed both r_p and $\Delta x/A_k$ to be independently varied. This led to anomalous effects, such as an apparent variation of $\Delta x/A_k$ with solute radius (Bowen et al., 1997). In reality, r_p and $\Delta x/A_k$ are linked through the membrane solvent permeability, and so their independent variation was physically inconsistent.

It is necessary to obtain pore inlet and outlet concentrations from the equilibrium partitioning expressions in order to calculate $c_{1,\mathrm{av}}$. The Donnan potential at the pore inlet ($x = 0$) is the same for both ions (although it differs from the potential at the pore outlet). Rearrangement of Eq. 7 and incorporation of partial partition coefficient Φ_i' gives:

$$\Delta\psi_D(0) = -\frac{RT}{F}\left[\ln\left(\frac{c_1(0)}{\Phi_1' C_w}\right)\right] = \frac{RT}{F}\left[\ln\left(\frac{c_2(0)}{\Phi_2' C_w}\right)\right] \tag{15}$$

Algebraic manipulation of Eq. 15 with Eq. 3 results in a quadratic partitioning expression, the solution of which can be expressed simply

$$c_1(0) = \frac{-X_d + \sqrt{X_d^2 + 4\Phi_1'\Phi_2' C_w^2}}{2} \tag{16}$$

Similarly, an equivalent quadratic expression at the pore outlet ($x = \Delta x$) gives

$$c_1(\Delta x) = \frac{-X_d + \sqrt{X_d^2 + 4\Phi_1'\Phi_2' C_p^2}}{2} \tag{17}$$

Special Case of KCl. KCl has been used in theoretical studies such as Bowen et al. (1997) and differs from other electrolytes through its near symmetry in terms of size and charge. For this electrolyte, if it is assumed that electrostatic interactions have little effect on the hindrance of ions in NF pores, then $K_{1,c} = K_{2,c} = K_c$, $D_{1,p} = D_{2,p} = D_p$, and $a_1 = a_2$ to a good approximation. (Such an assumption is used in all existing NF models, but its validity requires further investigation.) This allows the expressions just presented to be greatly simplified. Partitioning is also simplified for KCl because the partial partition coefficient is now the same for each ion. The potential gradient, from Eq. 9, becomes

$$\frac{F}{RT}\frac{d\psi}{dx} = -\frac{K_c V}{D_p}\frac{X_d}{2c_1 + X_d} \tag{18}$$

and Eq. 10 gives

$$\frac{\Delta c_1}{\Delta x} = \frac{VK_c}{D_p}\left[\left(c_{1,\mathrm{av}} - \frac{C_p}{K_c}\right) + \frac{c_{1,\mathrm{av}}X_d}{2c_{1,\mathrm{av}} + X_d}\right] \tag{19}$$

The equivalent expression for Eq. 14 is

$$C_p = \frac{K_c}{Pe}\left[c_{1,\mathrm{av}}Pe - \Delta c_1 + \frac{c_{1,\mathrm{av}}X_d}{2c_{1,\mathrm{av}} + X_d}Pe\right] \tag{20}$$

An important benefit of formulating the linearized system of equations is that the effect of X_d on overall rejection can be analyzed, as Eqs. 9, 11, 14, 16, and 17 are written in terms of X_d for the general case. The advantage of KCl is that this dependence can be assessed more readily in simplified expressions (Eqs. 18, 19, and 20). The importance of X_d in the analysis of experimental rejection using NF models has usually been discussed purely in terms of Donnan effects, although Eqs. 9 and 18 clearly show the effect of X_d on electromigrative transport to be important. Equations 14 and 20 make explicit the effect of X_d on permeate ion concentration.

Rejection of uncharged solutes

In the characterization of NF membranes, it is usual to obtain the pore radius, r_p, from the experimental rejection of uncharged solutes. The pore radius used in the linearized transport model for electrolyte rejection should, for consistency, have been obtained from an equivalent linearized model for uncharged solute rejection. The fundamental transport equation for uncharged solutes is the widely adopted hydrodynamic model, modified to include hindered convection and diffusion within the pores, as proposed by Anderson and Quinn (1974) and Deen (1987), where solute concentration gradient is defined as

$$\frac{dc}{dx} = \frac{V}{D_p}(K_c c - C_p) \tag{21}$$

It is worth noting that this expression differs from the corresponding expression for ions (Eq. 6) only through the lack of an electromigrative term. The linearized concentration gradient can be expressed simply as

$$\frac{\Delta c}{\Delta x} = \frac{K_c V}{D_p}\left(c_{\text{av}} - \frac{C_p}{K_c}\right) \tag{22}$$

Introduction of the Peclet number as before gives

$$C_p = \frac{K_c}{Pe}(c_{\text{av}} Pe - \Delta c) \tag{23}$$

Substitution for c_{av} and Δc in Eq. 23 (using steric partitioning to relate bulk solute concentrations to pore inlet and outlet concentrations) and definition of rejection R gives

$$R = 1 - \frac{C_p}{C_w} = \frac{1 - \Phi K_c}{\left(1 - \frac{\Phi K_c}{2}\right) + \frac{\Phi K_c}{Pe}} \tag{24}$$

This differs from the analytical solution of Eq. 21 (the full model), which gives

$$R = 1 - \frac{\Phi K_c}{1 - [1 - \Phi K_c]\exp(-Pe)} \tag{25}$$

A simple way to characterize the pore radius of a membrane is through the limiting rejection, where convective transport dominates and rejection, in the limiting case $Pe \to \infty$, is only dependent on pore radius. The predicted limiting rejection in the linearized model differs from that of the full model, $R_{\text{lim}} = 1 - \Phi K_c$, through an additional term in the denominator of Eq. 24

$$R_{\text{lim}} = \frac{1 - \Phi K_c}{1 - 0.5\Phi K_c} \tag{26}$$

Discrepancies between the pore radii obtained from the analysis of uncharged solute rejection with both the full and linearized models are greatest for the case of limiting rejection. The effect of the first-order term in Eq. 21 (which introduces nonlinearity in the concentration profiles) increases with solvent velocity, which is infinitely large in the case of limiting rejection.

Calculation procedure and characterization of NF membranes

The system of equations described by the full model has been reduced, through linearization of the concentration gradient, to three independent equations in three unknowns, namely $c_1(0)$, $c_1(\Delta x)$, and C_p. The overall iterative solution method for this system can be performed simply, using a spreadsheet, for any value of X_d:

(1) Calculate $c_1(0)$ using Eq. 16 and the known feed concentration C_w.

(2) Estimate a value of C_p and calculate $c_1(\Delta x)$ using Eq. 17.

(3) Calculate $c_{1,\text{av}}$ and Δc_1 using Eq. 12 and check the guess for C_p using Eq. 14.

(4) Iterate C_p using a simple bracketing method such as bisection or false position, since $0 \le C_p \le C_w$. Terminate when $C_p\ (\textit{Iteration}) = C_p$ (Eq. 14).

(5) Calculate rejection R from the usual definition, $R = 1 - (C_p/C_w)$.

A significant advantage for uni-univalent electrolytes in this simplified approach is that the partitioning expressions reduce to a quadratic equation that can be solved simply. The introduction of multivalent ions would lead to a requirement for solution of cubic and higher-order expressions with the Newton–Raphson method.

The major advantage of the linearization method over analytical solution of the extended Nernst–Planck equation is that it is possible to extend this approach to multicomponent electrolytes. In such cases, the transport equations are reduced to a system of $n-1$ simultaneous equations. (The appropriate linearized equations are derived in full for a ternary-ion system in the Appendix.) For multivalent ions, it is no longer possible to obtain explicit expressions for permeate concentrations but such concentrations can be obtained by iteration, as discussed in the Appendix.

The first requirement in analysis of NF processes is often to characterize the membrane. This may be achieved using the linearized model as follows:

(1) Analyze uncharged solute rejection data as a function of ΔP_e using Eq. 24 in order to obtain pore radius, r_p.

(2) Assess the average pore dielectric constant, ϵ_p, by least-square fitting of Eqs. 7, 8 in the analysis of electrolyte (most usually NaCl) rejection as a function of ΔP_e at the membrane isoelectric point (pH giving the minimum electrolyte rejection).

(3) Investigate the charging properties of the membrane through evaluation of effective membrane charge density, X_d, from the variation of electrolyte (NaCl) rejection with concentration.

(4) If predictions of flux properties are required, as in diafiltration, then they can be evaluated simply from the solvent permeability, L_p (accounting, if necessary, for concentration polarization in evaluating ΔP_e).

The procedure just described is for membranes that exhibit an isoelectric point within the accessible range of operating pH. In such cases, the use of electrolyte rejection at the membrane isoelectric point enables dielectric mechanisms to be decoupled from Donnan effects. It is also well known that Donnan effects significantly decrease with increasing electrolyte concentration. So, for membranes without an accessible isoelectric point, it is feasible to assess pore dielectric constant using rejection data at higher salt concentrations, for example, 0.1 M NaCl, and assuming that X_d is negligible at such a concentration. The use of an even higher concentration would introduce significant nonideality in solution behavior.

The system of equations just proposed are derived for transport in any NF pore but, because of excellent feed-side mass transfer in the pilot-scale experimentation used in the present study, are not extended to include concentration polarization phenomena. Under polarization conditions, the wall concentrations in Eqs. 15, 16 and 24 can be adjusted through the use of either an appropriate mass-transfer correlation or solution of the extended Nernst–Planck equation in the feed-side boundary layer, as performed by Bowen and Mohammad (1998).

Experimental Methods

Memtech (UK) Ltd. constructed the pilot-scale apparatus used in this study. A spiral-wound NF module was used in all experiments, containing 1.7 m^2 of Desal-DK (Osmonics-Desal) membrane. Flexibility of operation was obtained through the use of two pumps, a diaphragm pump supplying the high pressures to the system, and a centrifugal pump generating the high cross-flows.

The volumetric flows of both permeate (which was converted to flux) and retentate streams were measured using electromagnetic flowmeters. The pressures of the feed (module inlet), retentate, and permeate streams were measured to within ± 0.01 MPa using diaphragm-type transmitters. The system temperature was controlled to within ± 0.2°C by regulating the flow of cooling water to a heat exchanger.

For ionic solutes, a simple technique for measuring concentration is through the conductivity of the solution. Conductivity measurements were made of the permeate and retentate streams using double-electrode probes capable of measuring conductivities ranging from 5 $\mu S \cdot cm^{-1}$ to 300 mS $\cdot cm^{-1}$. Sodium and chloride ion concentrations were measured with an ion-selective probe (Russell pH), individual ion concentrations being calculated using a combination of these measurements and total solution conductivity.

The measured process data were continuously logged using a PC, any noise in the data being smoothed with a moving-average statistical treatment of the data. In all of the experiments performed, rejection was measured at pressures ranging from 0.1 MPa to 2.5 MPa. Preliminary experimentation with the NF module showed that concentration polarization was very small. Initially, the rejection of NaCl was measured as a function of volumetric cross-flow, Q, where rejection was found to be only weakly dependent on cross-flow at the flows used in the filtration experiments in the present work. These data were analyzed using a velocity variation method analogous to that of Nakao and Kimura (1981) using the assumption that $k \propto Q^{0.875}$ for turbulent flow in spiral-wound modules (Schock and Miguel, 1987). This analysis showed that the observed rejection at the highest operating pressure was within 4% of the polarization-corrected rejection ($Q \rightarrow \infty$). The correction at lower pressures was smaller.

In the models proposed in this study, rejection is predicted as a function of effective pressure, ΔP_e, and so it is necessary to correct experimental applied pressure by the osmotic pressure. Electrolyte rejection was studied over a range of concentrations, and so osmotic pressure corrections were made using the van't Hoff equation (Bowen and Mohammad, 1998), which was applicable since concentrations did not exceed 0.1 M.

Table 1. Pore Radii from Analysis of Uncharged Solute Rejection Data with Both Full and Linearized One-Parameter Models

	Full Model		Linearized Model	
	r_p (nm)	S_y	r_p (nm)	S_y
Glycerol	0.45	0.026	0.45	0.026
Glucose	0.43	0.006	0.44	0.005
Overall	0.45	0.025	0.45	0.025

Throughout this study, it was necessary to compare the agreement with experimental data of the full and linearized models. The quality of fit was compared through the following least-square objective function S_y

$$S_y = \sqrt{\frac{\sum_1^n \left(R_{\text{exp}} - R_{\text{calc}}\right)^2}{n-1}} \tag{27}$$

Results and Discussion

Characterization of the Desal-DK membrane

Experimental uncharged solute rejection data were analyzed with the linearized one-parameter transport model (Eq. 24). The effective pore radii obtained were compared to those obtained from analysis of the data with the full one-parameter model (Eq. 25). Table 1 presents a summary of the fittings, showing that the results for pore radius and S_y were in close agreement. Figure 1 illustrates the agreement to experimental data, which is comparable for both models. A pore

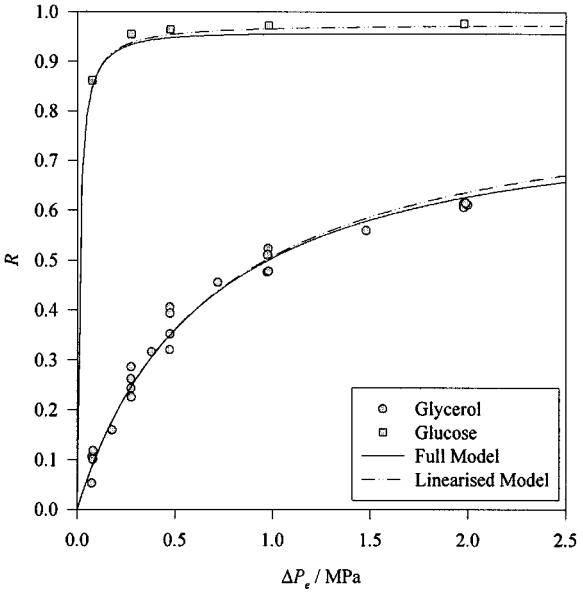

Figure 1. Fits from experimental uncharged solute rejection data with both full and linearized one-parameter models.

Glycerol rejection was measured in both water and various NaCl solutions (from 0.001 M to 0.1 M). Desal-DK membrane.

radius $r_p = 0.45$ nm will therefore be used in all subsequent analysis of experimental data with either model.

The experimental rejection of 0.01 M NaCl at the Desal-DK membrane was determined over a range of pH and was found to exhibit a minimum at pH ~4.1, this phenomenon being attributed to the membrane being at its isoelectric point. This observation of zero effective charge at pH ~4.1 was in agreement with zeta-potential studies of this membrane (Hagmeyer and Gimbel, 1998). The average pore dielectric constant was estimated, using the linearized three-parameter model, to be $\epsilon_p \sim 38$ at this pore radius—the same value as that obtained from analysis with the full model, further justifying the linear assumption. This pore dielectric constant was used in all comparisons to experimental electrolyte rejection data for this membrane. However, the concentration gradient within the pore also depends on X_d, and so the validity of linearization was tested at nonisoelectric conditions.

Experimental NaCl rejection data for the Desal-DK membrane has been analyzed using the full and linearized three-parameter models. A summary of best fits obtained for the variation of NaCl rejection with concentration is shown in Table 2 where, again, fitting results are in very close agreement. Figure 2 gives a graphical presentation of the best fits obtained with both models, where the differences between the two models are indistinguishable. Table 2 shows a systematic increase in the magnitude of X_d as C_w increases from 1.4 to 37.6 mol^{-3}. This is consistent with anion adsorption at the membrane, as has been previously found for a number of nanofiltration membranes. However, X_d shows a decrease in magnitude at $C_w = 111.8$ mol^{-3}. This could possibly be explained by either the adsorption of cations at the higher concentration or by a change in the dielectric properties of pore water with increasing salt concentration (which is not included in the model for pore dielectric constant in the present article).

The procedure described in the subsection titled "Calculation procedure and characterization of NF membranes" using 0.1 M NaCl in the assessment of pore dielectric constant was also performed (the data are not presented here). The agreement to experimental data was comparable to that in Figure 2 at all concentrations, although the predicted X_d values were greater in magnitude.

Range of validity of linearized concentration gradients

The characterization of a small-pore-size NF membrane in this has shown the linearization of the concentration gradient to be valid for both uncharged solutes and single electrolytes.

Table 2. Effective Charge Densities from Analysis of NaCl Rejection Data with Full and Linearized Three-Parameter Models

	Full Model			Linearized Model		
C_w (mol·m^{-3})	X_d (mol·m^{-3})	ξ	S_y	X_d (mol·m^{-3})	ξ	S_y
1.4	−0.49	−0.35	0.033	−0.50	−0.36	0.033
3.7	−1.07	−0.29	0.038	−1.07	−0.29	0.038
11.0	−2.07	−0.19	0.038	−2.05	−0.19	0.038
37.6	−5.73	−0.15	0.060	−5.75	−0.15	0.059
111.8	−1.89	−0.02	0.052	−1.85	−0.02	0.053

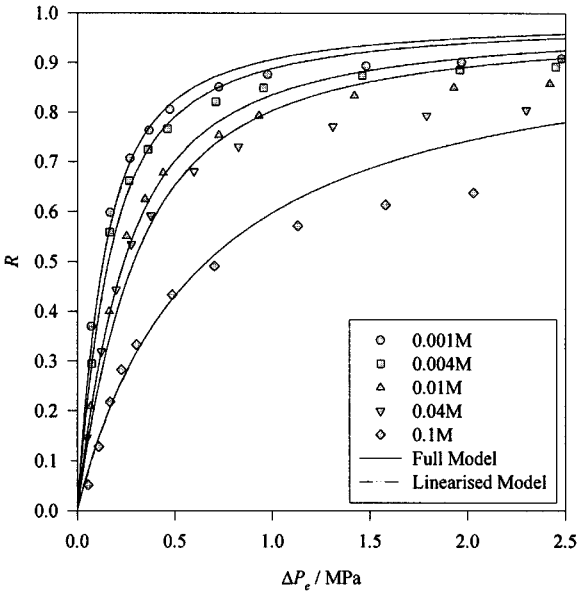

Figure 2. Fits from experimental NaCl rejection data with both full and linearized three-parameter models ($r_p = 0.45$ nm) with reassessed dielectric exclusion: Desal-DK membrane.

However, the characteristics of NF membranes vary quite considerably, and so the validity of this procedure must be tested over a wider range of NF conditions. Theoretical simulations were performed with the full model in order to evaluate the ion-concentration profiles within NF pores. As stated earlier, the concentration gradients are also dependent on X_d, and so the NaCl concentration profiles were investigated over a range of both pore radius ($0.5 < r_p < 2.0$ nm) and membrane charge, Figure 3.

It was necessary to estimate pore dielectric constant as a function of pore radius. The solvent within the pores was assumed to consist of one layer of oriented water molecules with a dielectric constant, ϵ^*, and an inner part having bulk dielectric properties. This assumption of pore solvent structure is in agreement with previous electrochemical studies of colloid–solvent interfaces (Israelachvili, 1991) and NMR studies of the relaxation of water adsorbed on glass surfaces (Belfort et al., 1974). The variation of the average pore dielectric constant can then be calculated on a geometric basis (assuming $\epsilon_b = 80$)

$$\epsilon_p = 80 - 2(80 - \epsilon^*)\left(\frac{d}{r_p}\right) + (80 - \epsilon^*)\left(\frac{d}{r_p}\right)^2 \qquad (28)$$

This evaluation allows a quasi-continuum-level exploration of the effects of a variation of pore solvent dielectric constant that may be used for predictive purposes. Further theoretical improvements could probably only be achieved through noncontinuum descriptions, such as molecular dynamic simulations, with considerable increase in conceptual and computational requirements. Using the data for the Desal-DK membrane, it is possible to estimate that the dielectric constant for the oriented water layer has a value $\epsilon^* \sim 31$, allowing the

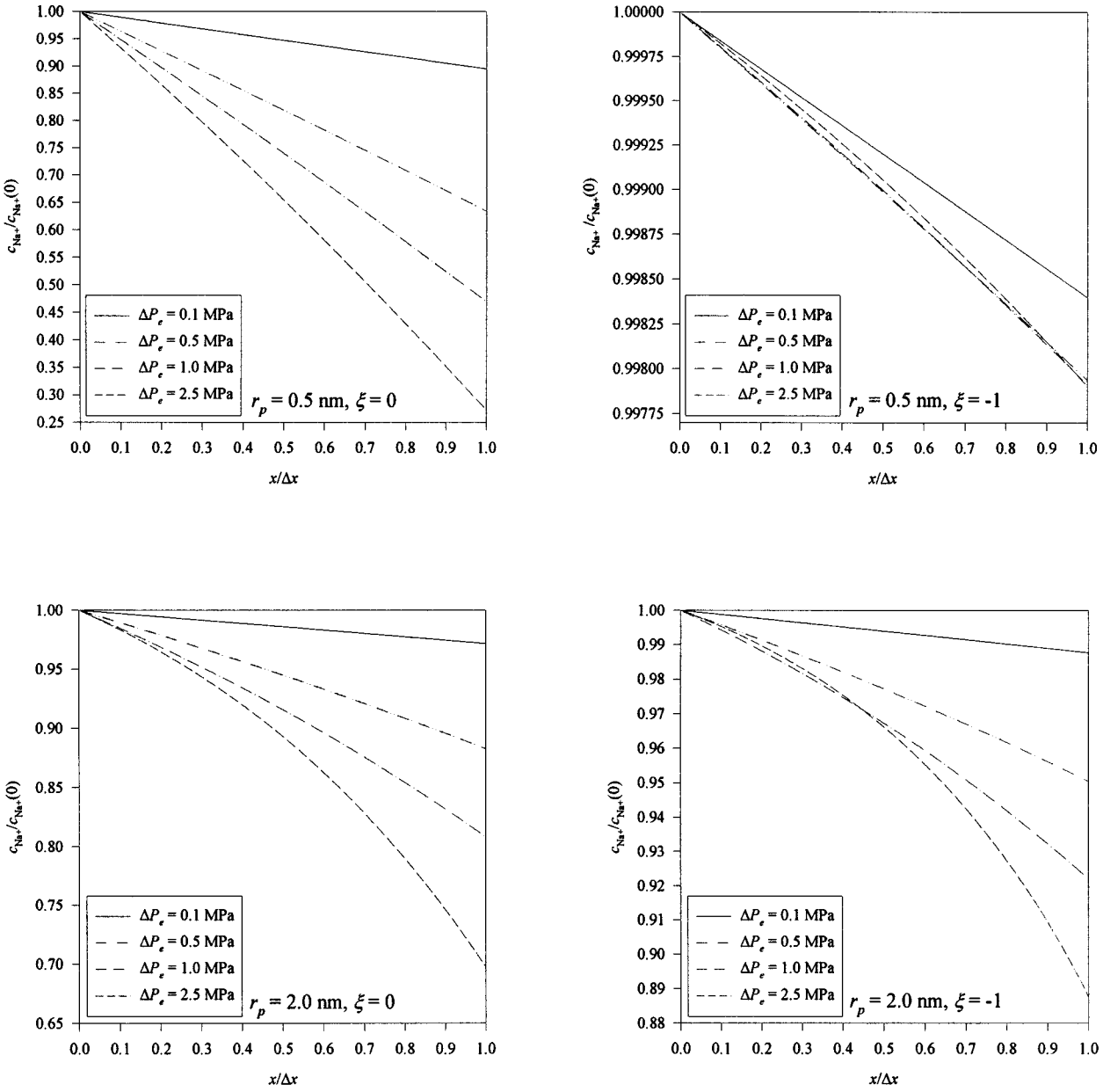

Figure 3. Theoretical dimensionless Na^+ ion concentrations for rejecting NaCl over a range of pore radius and ratio of membrane charge density to bulk feed concentration, ξ.

average pore dielectric constants for pores of $r_p = 0.5$ and 2.0 nm to be estimated as $\epsilon_p \sim 40$ and 67, respectively.

The dimensionless Na^+ ion concentration profiles in Figure 3 have been normalized with the pore inlet concentration. The corresponding Cl^- ion profiles are not included here because, for single electrolytes, electroneutrality within pores forces the concentration profiles to be parallel. The profiles in Figure 3 show excellent linearity at the smaller pore radius, although curvature is greater at the larger charge density. This linearity explains the excellent agreement between the full and linearized models during the characterization of the Desal-DK membrane. For $r_p = 2.0$ nm the curvature is more apparent, though only really significantly at the highest pressure ($\Delta P_e = 2.5$ MPa). Such a pore radius corresponds to an upper limit for nanofiltration membranes.

It can be concluded, therefore, that the linearization of concentration gradients in the transport of single electrolytes will be reasonably valid over the range of NF pore sizes. As a further test, Figure 4 shows the predicted rejection of NaCl at various ξ values for both the linearized and full models for $r_p = 2.0$ nm. Even over such an extended range of ξ, there is very good agreement between the calculations.

The linearization of the concentration gradient is valid when the effect of the c^2 term in Eqs. 10, 19, A9, and A10 is small. All three variables in the ion-specific group K_cV/D_p exhibit a strong radius dependence, although in general terms

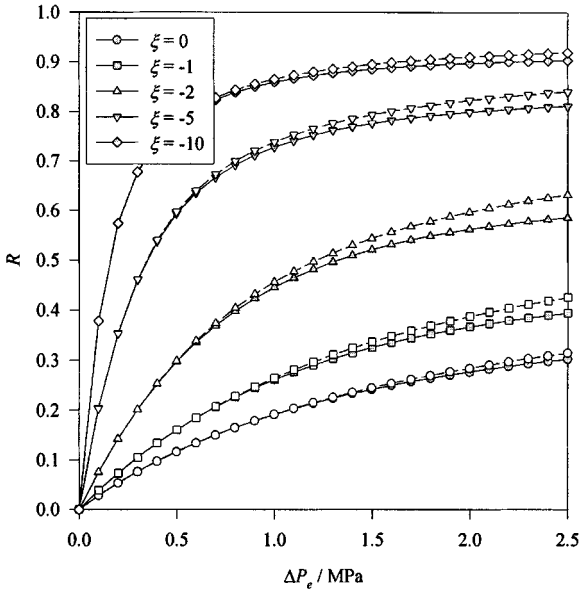

Figure 4. Theoretical variation of NaCl rejection with the ratio of membrane charge density to bulk feed concentration, ξ, for both full and linearized models (r_p = 2.0 nm).

Grey symbols—full model, white symbols—linearized model.

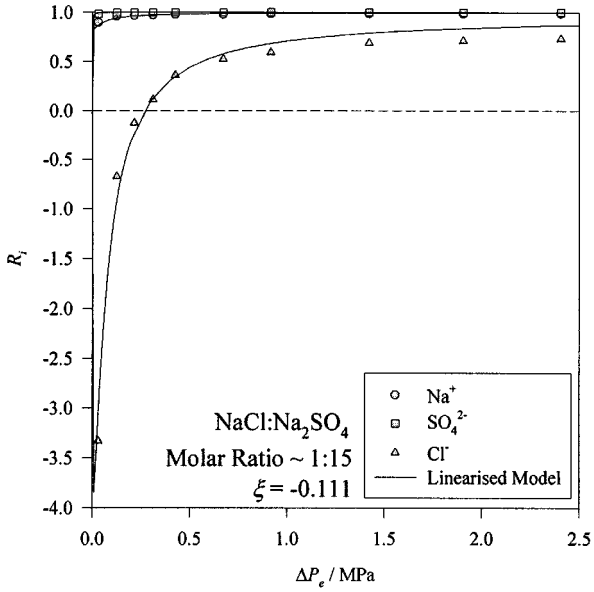

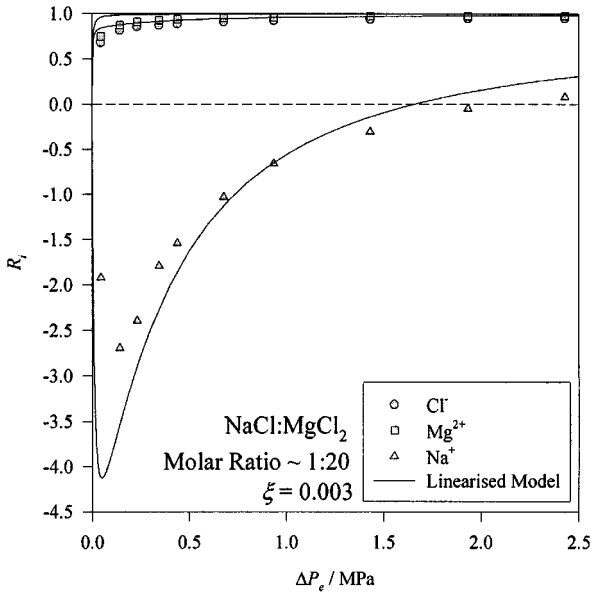

Figure 5. Fits from experimental rejection of NaCl: Na_2SO_4 and NaCl:$MgCl_2$ mixtures with linearized model (r_p = 0.45 nm): Desal-DK membrane.

the effects of hindrance factors (through K_c and D_p) will be greater in the smaller NF pores and the effect of solvent velocity greater for larger pores, so that there is some cancellation of the effects. Nevertheless, the dependence on V results in the increase of the concentration profile curvature with increasing ΔP_e. However, a very important feature of the success of linearization lies in the effect of dielectric exclusion, which is also a pore-size-dependent phenomenon. Pore-ion concentrations are reduced since both coions and counterions are excluded, and in particular, counterion concentrations are smaller than in previous models because of the smaller values of X_d. In many cases, therefore, the magnitude of c^2 may be negligible irrespective of the value of K_cV/D_p.

Rejection of ternary electrolytes mixtures

Electrolyte mixtures have sometimes been used as a test system in the development of predictive NF models (Tsuru et al., 1991b; Rios et al., 1996). The linearized model described in the Appendix was therefore used to investigate the rejection of NaCl:Na_2SO_4 and NaCl:$MgCl_2$ mixtures. The phenomenon of negative rejection was observed in both mixtures, the magnitude of this negative rejection increasing with the ratio of divalent to monovalent coion. The agreement with the experimental data obtained with the linearized model is shown in Figure 5 for the systems that exhibited the largest negative rejections (the fit again being indistinguishable from that of the full model). Pore ion concentration profiles are no longer parallel in the case of electrolyte mixtures, as presented in Figure 6 for NaCl:Na_2SO_4 mixtures under conditions corresponding to those of maximum curvature in Figure 3. The profiles show significant curvature at the highest pressure, although it is important to recognize that these curves represent conditions where the deviation from linearity will be near its maximum under practical NF conditions.

Figure 6 also shows that the axial variations in dimensionless Cl^- and SO_4^{2-} concentration can be significant. Further model sophistication could result from the inclusion of an axial variation in X_d. However, such a development would cause a significant increase in the mathematical complexity of the model (and would also ideally require a reliable description for the development of charge at membranes where a detailed knowledge of the surface chemistry is rarely available).

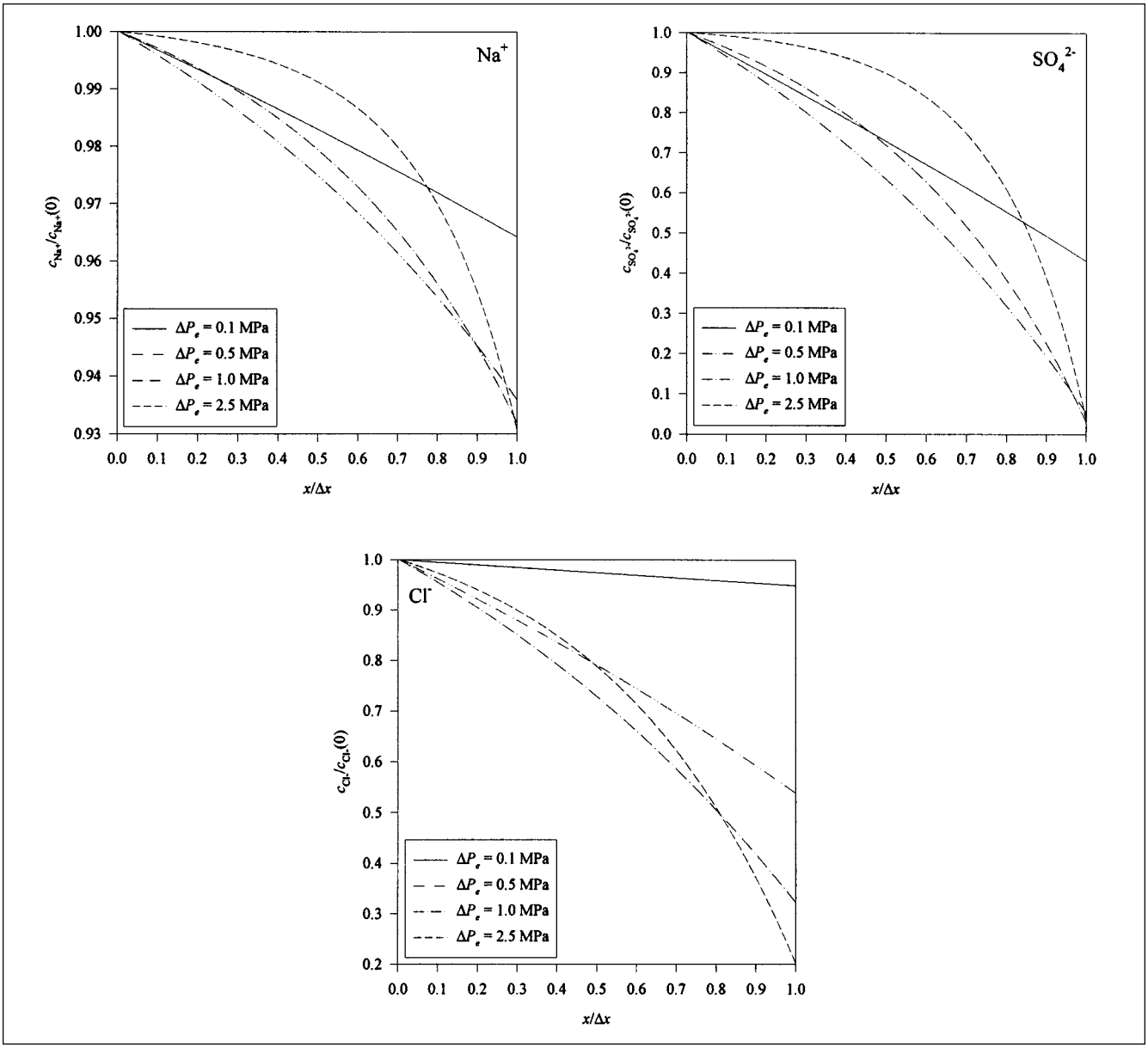

Figure 6. Theoretical dimensionless ion concentrations for rejecting NaCl:Na_2SO_4 mixtures.

$r_p = 2.0$ nm, $\xi = -1$, molar ratio = 1:10.

Overall, the linearization of the concentration gradients in the three-parameter model is reasonably valid over the entire NF range of conditions, predictions of single and multicomponent electrolyte rejection being identical to the fall model in narrow pores ($r_p \sim 0.5$ nm).

Conclusions

Finite difference linearization of the pore concentration gradient in nanofiltration membranes has been shown to greatly simplify the solution of a three-parameter model for electrolyte rejection through removal of the need for numerical Runge–Kutta integration of the extended Nernst–Planck equation. The proposed linearized model also differs from previous models through the simultaneous introduction of dielectric exclusion in the equilibrium partitioning at the pore inlet and outlet and the removal of the ratio of effective membrane thickness to porosity ($\Delta x/A_k$), which serves purely as a fitting parameter. The effect of dielectric exclusion on electrolyte rejection must, at this stage in model development, be assessed from experimental salt rejection data and so pore dielectric constant acts as the third model parameter.

The validity of the linearized model is first proved experimentally through comparison with the results obtained with the full model during the rigorous characterization of a small-pore-size NF membrane. The two models were seen to very closely agree, and subsequent analysis of pore concentration profiles suggested that the assumption of linearity would always be valid for practical purposes in such small pores ($r_p = 0.45$ nm). This agreement allowed a computa-

tionally simple characterization procedure to be proposed that employs the linearized model as a practical tool in preliminary studies of NF membranes (including an alternative approach to the assessment of pore dielectric constant using the rejection of 0.1 M NaCl).

Further investigation of pore concentration profiles showed the assumption of linearity to be valid over a wide range of practical NF conditions, demonstrating the importance of dielectric exclusion in reducing both the magnitude of X_d and the coion concentrations within the pore. The linearized model was also successfully extended to ternary electrolyte mixtures, highlighting its main advantage over analytic solutions that are limited to univalent electrolytes.

Overall, the model described in the present article is a powerful tool for the characterization of NF membranes and subsequent prediction of separation performance due to the removal of the need for complex nonlinear numerical methods through the reduction of the governing equations to a system of algebraic expressions. In addition, linearization reduces the calculation time required to generate predictions for the rejection of multicomponent solutions by at least two orders of magnitude.

Acknowledgments

We thank the UK Engineering and Physical Sciences Council and the UK Biotechnology and Biological Sciences Research Council for funding this work, and Avecia for a CASE studentship for JSW.

Notation

a_i, a = hydrodynamic (Stokes) radius of ion i or KCl ions, m
A = function defined by Eq. A3, m^{-1}
A_k = porosity, dimensionless
B = function defined by Eq. A3, m^{-1}
c_i, c = concentration of ion i or uncharged solute within pore, $mol \cdot m^{-3}$
$c_i(0), c(0)$ = concentration of ion i or uncharged solute within pore entrance, $mol \cdot m^{-3}$
$c_i(\Delta x), c(\Delta x)$ = concentration of ion i or uncharged solute within pore outlet, $mol \cdot m^{-3}$
$c_{i,av}, c_{av}$ = average concentration of ion i or uncharged solute within pore, $mol \cdot m^{-3}$
C_f = bulk feed concentration, $mol \cdot m^{-3}$
$C_{i,p}, C_p$ = permeate concentration of ion i or uncharged solute, $mol \cdot m^{-3}$
$C_{i,w}, C_w$ = wall concentration of ion i or uncharged solute, $mol \cdot m^{-3}$
$D_{i,p}, D_p$ = pore diffusion coefficient of ion i or uncharged solute, $m^2 \cdot s^{-1} (= K_{i,d} D_\infty)$
$D_{i,\infty}, D_\infty$ = bulk diffusion coefficient of ion i or uncharged solute, $m^2 \cdot s^{-1}$
d = thickness of the oriented solvent layer, m
e = electronic charge, 1.602177×10^{-19} C
E = function defined by Eq. A3, m^{-1}
f_i = iterative method test function for ion i, $mol \cdot m^{-3}$
f_T = overall iterative method test function, $mol \cdot m^{-3}$
F = Faraday constant, 96487 $C \cdot mol^{-1}$
G = function defined by Eq. A3, m^{-1}
H = function defined by Eq. A3, m^{-1}
j_i = ionic flux of ion i (pore area basis), $mol \cdot m^{-2} \cdot s^{-1}$
J = function defined by Eq. A3, dimensionless
J_v = volumetric flux, $m^3 \cdot m^{-2} \cdot s^{-1}$
k = Boltzmann constant, 1.38066×10^{-23} $J \cdot K^{-1}$
k = feed-side mass-transfer coefficient, $m \cdot s^{-1}$
$K_{i,c} K_c$ = hindrance factor for convection of ion i or uncharged solute, dimensionless, $[K_c = (2 - \Phi)(1.0 + 0.054\lambda - 0.988\lambda^2 + 0.441\lambda^3)]$ (Bowen and Mohammad, 1998)
$K_{i,d}, K_d$ = hindrance factor for diffusion of ion i or uncharged solute, dimensionless, $(K_d = 1.0 - 2.30\lambda + 1.154\lambda^2 + 0.224\lambda^3)$ (Bowen and Mohammad, 1998)
L = function defined by Eq. A3, dimensionless
M = function defined by Eq. A3, dimensionless
n = number of solutes in fitting, dimensionless
P = function defined by Eq. A6, m^{-1}
Pe_i, Pe = Peclet number for ion i or uncharged solute, dimensionless
Q = volumetric cross-flow rate in the spiral wound module, $m^3 \cdot s^{-1}$
Q = function defined by Eq. A6, m^{-1}
r_p = effective pore radius, m
R, R_i = rejection of electrolyte or ion i, dimensionless
R = universal gas constant, 8.314 $J \cdot mol^{-1} \cdot K^{-1}$
R_{calc} = calculated rejection, dimensionless
R_{exp} = experimental rejection, dimensionless
R_{lim} = limiting rejection, dimensionless
$S_1 \rightarrow S_7$ = functions defined by Eq. A6, m^{-1}
S_y = sum-of-squares objective function in fitting, dimensionless
T = absolute temperature, K
$T_1 \rightarrow T_7$ = functions defined by Eq. A8, m^{-1}
U = function defined by Eq. A8, m^{-1}
V = solvent velocity (defined by Hagen–Poiseuille), $m \cdot s^{-1}$
x = axial position within the pore, m
X_d = effective charge density, $mol \cdot m^{-3}$
Y = function defined by Eq. A8, m^{-1}
z_i = valence of ion i, dimensionless

Greek letters

$\Delta c_i, \Delta c$ = concentration difference of ion i or uncharged solute across the pore thickness, $mol \cdot m^{-3}$
ΔP = applied pressure, $N \cdot m^{-2}$
ΔP_e = effective pressure driving force, $N \cdot m^{-2}$ $(\Delta P_e = \Delta P - \Delta \pi)$
$\Delta \pi$ = dynamic osmotic pressure difference, $N \cdot m^{-2}$ $(\Delta \pi = RT[\Sigma C_{i,w} - \Sigma C_{i,p}])$
ΔW_i = Born solvation energy barrier, J
Δx = membrane thickness, m
$\Delta \psi_{i,D}(0)$ = Donnan potential of ion i at the pore entrance, V
ϵ_b = bulk dielectric constant, dimensionless
ϵ_p = pore dielectric constant, dimensionless
ϵ_o = permittivity of free space, 8.85419×10^{-12} $J^{-1} \cdot C^2 \cdot m^{-1}$
ϵ_b = dielectric constant of the oriented water layer, dimensionless
η = solvent viscosity within pores, $N \cdot s \cdot m^{-2}$
λ = ratio of ionic or uncharged solute radius to pore radius, dimensionless
ξ = ratio of effective membrane charge density to bulk feed concentration, dimensionless $(\xi = X_d/C_f)$
Φ_i' = partial partition coefficient, dimensionless $(\Phi_i' = \Phi_i \exp[-\Delta W_i/kT])$
Φ_i, Φ = steric partition coefficient of ion i or uncharged solute, dimensionless, $= (1 - \lambda)^2$
ψ = potential within the pore, V

Literature Cited

Acton, F. S., *Numerical Methods That Work*, Harper & Row, New York (1970).

Afonso, M. D., and M. N. de Pinho, "Transport of $MgSO_4$, $MgCl_2$ and Na_2SO_4 Across an Amphoteric Nanofiltration Membrane," *J. Memb. Sci.*, **179**, 137 (2000).

Anderson, J. L., and J. A. Quinn, "Restricted Transport in Small Pores: A Model for Steric Exclusion and Hindered Particle Motion," *Biophys. J.*, **14**, 130 (1974).

Belfort, G., J. Scherig, and D. O. Seevers, "Nuclear Magnetic Resonance Relaxation Studies of Adsorbed Water on Porous Glass of Varying Sizes," *J. Colloid Interface Sci.*, **47**, 106 (1974).

Born, M., "Volumen and hydratationswärme der Ionen," *Z. Phys. Chem.*, **1**, 45 (1920).

Bowen, W. R. and F. Jenner, "Electroviscous Effects in Charged Capillaries," *J. Colloid Interface Sci.*, **173**, 388 (1995).
Bowen, W. R., A. W. Mohammad, and N. Hilal, "Characterisation of Nanofiltration Membranes for Predictive Purposes—Use of Salts, Uncharged Solutes and Atomic Force Microscopy," *J. Memb. Sci.*, **126**, 91 (1997).
Bowen, W. R., and A. W. Mohammad, "Diafiltration by Nanofiltration: Prediction and Optimization," *AIChE J.*, **44**, 1799 (1998).
Combe, C., C. Guizard, P. Aimar, and V. Sanchez, "Synthesis and Characterization of Microporous Zirconia Powders: Application in Nanofilters and Nanofiltration Characteristics," *J. Memb. Sci.*, **132**, 109 (1997).
Deen, W. M., "Hindered Transport of Large Molecules in Liquid-Filled Pores," *AIChE J.*, **33**, 1409 (1987).
Dresner, L., "Some Remarks on the Integration of Extended Nernst-Planck Equation in the Hyperfiltration of Multicomponent Solutions," *Desalination*, **10**, 27 (1972).
Fane, A. G., A. R. Awang, M. Bolko, R. Macoun, R. Schofield, Y. R. Shen, and F. Zha, "Metal Recovery from Wastewater Using Membranes," *Water Sci. Technol.*, **25**, 5 (1992).
Hagmeyer, G., and R. Gimbel, "Modelling the Salt Rejection of Nanofiltration Membranes for Ternary Ion Mixtures and for Single Salts at Different pH Values," *Desalination*, **117**, 247 (1998).
Hoffer, L., H. Schwinn, L. Biesert, and D. Josic, "Improved Virus Safety and Purity of a Chromatographically Produced Factor-IX Concentrate by Nanofiltration," *J. Chromatog. B-Bio. Appl.*, **669**, 187 (1995).
Israelachvili, J. N., *Intermolecular and Surface Forces*, 2nd ed., Academic Press, London (1991).
Nakao, S., and S. Kimura, "Analysis of Solutes Rejection in Ultrafiltration," *J. Chem. Eng. Jpn.*, **14**, 32 (1981).
Rios, G. M., R. Joulie, S. J. Sarrade, and M. Carles, "Investigation of Ion Separation by Microporous Nanofiltration Membranes," *AIChE J.*, **42**, 2521 (1996).
Rosa, M. J., and M. N. de Pinho, "The Role of Ultrafiltration and Nanofiltration on the Minimization of the Environmental-Impact of Bleached Pulp Effluents," *J. Memb. Sci.*, **102**, 155 (1995).
Saksena, S., and A. L. Zydney, "Pore Size Distribution Effects on Electrokinetic Phenomena in Semipermeable Membranes," *J. Memb. Sci.*, **105**, 203 (1995).
Sarrade, S., G. M. Rios, and M. Carles, "Dynamic Characterisation and Transport Mechanisms of Two Inorganic Membranes for Nanofiltration," *J. Memb. Sci.*, **97**, 155 (1994).
Schlögl, R., "Membrane Permeation in Systems Far from Equilibrium," *Ber. Bunsenges. Phys. Chem.*, **70**, 400 (1966).
Schock, G., and A. Miguel, "Mass Transfer and Pressure Loss in Spiral Wound Modules," *Desalination*, **64**, 339 (1987).
Tsuru, T., M. Urairi, S. Nakao, and S. Kimura, "Reverse Osmosis of Single and Mixed Electrolytes with Charged Membranes: Experiment and Analysis," *J. Chem. Eng. Jpn.*, **24**, 518 (1991a).
Tsuru, T., S. Nakao, and S. Kimura, "Calculation of Ion Rejection by Extended Nernst-Planck Equation with Charged Reverse Osmosis Membranes for Single and Mixed Electrolyte Solutions," *J. Chem. Eng. Jpn.*, **24**, 511 (1991b).
Tsuru, T., T. Shutou, S. Nakao, and S. Kimura, "Peptide and Amino Acid Separation with Nanofiltration Membranes," *Sep. Sci. Technol.*, **29**, 971 (1994).
van der Horst, H. C., J. M. K. Timmer, T. Robbertsen, and J. Leenders, "Use of Nanofiltration for Concentration and Demineralization in the Dairy Industry: Model for Mass Transport," *J. Memb. Sci.*, **104**, 205 (1995).
Wang, X. L., T. Tsuru, M. Togoh, S. Nakao, and S. Kimura, "The Electrostatic and Steric-Hindrance Model for the Transport of Charged Solutes Through Nanofiltration Membranes," *J. Memb. Sci.*, **135**, 19 (1997).
Wesselingh, J. A., and R. Krishna, *Mass Transfer in Multicomponent Mixtures*, Delft Univ. Press, Delft, The Netherlands (2000).

Appendix: Derivation of Linearized Transport Equations for Electrolyte Mixtures

It is possible to extend this linearization procedure to the transport of three ions in NF pores. The transport equations will be derived for a general three-ion system and then the partitioning of two common systems will be examined (Na^+:SO_4^{2-}:Cl^- and Cl^-:Mg^{2+}:Na^+). The full model potential gradient, Eq. 2, is thus extended as follows

$$\frac{d\psi}{dx} = \frac{\frac{z_1 V}{D_{1,p}}\left(K_{1,c}c_1 - C_{1,p}\right) + \frac{z_2 V}{D_{2,p}}\left(K_{2,c}c_2 - C_{2,p}\right) + \frac{z_3 V}{D_{3,p}}\left(K_{3,c}c_3 - C_{3,p}\right)}{\frac{F}{RT}\left(z_1^2 c_1 + z_2^2 c_2 + z_3^2 c_3\right)} \quad \text{(A1)}$$

It is possible to substitute for ion 3 using electroneutrality conditions (as was performed for ion 2 earlier, in the case of single electrolytes). Introduction of these expressions into Eq. A1 allows the potential gradient to be defined in terms of c_1, c_2, $C_{1,p}$, $C_{2,p}$, and X_d

$$\frac{F}{RT}\frac{d\psi}{dx} = \frac{Ac_1 + Bc_2 - EC_{1,p} - GC_{2,p} - HX_d}{Jc_1 + Lc_2 - MX_d}, \quad \text{(A2)}$$

where

$$A = z_1 V\left(\frac{K_2}{D_{1,p}} - \frac{K_3}{D_{3,p}}\right), \qquad B = z_2 V\left(\frac{K_2}{D_{2,p}} - \frac{K_3}{D_{3,p}}\right),$$

$$E = z_1 V\left(\frac{1}{D_{1,p}} - \frac{1}{D_{3,p}}\right),$$

$$G = z_2 V\left(\frac{1}{D_{2,p}} - \frac{1}{D_{3,p}}\right), \qquad H = \frac{K_{3,c}V}{D_{3,p}},$$

$$J = z_1^2 - z_1 z_3, \qquad L = z_2^2 - z_2 z_3, \qquad M = z_3 \quad \text{(A3)}$$

For a system of three ions, there are $n-1$ independent concentration gradients, and so it is necessary to derive expressions for ions 1 and 2 only. Substitution of Eq. A2 into the concentration gradient for ion 1, Eq. 6, yields

$$\frac{dc_1}{dx} = \frac{V}{D_{1,p}}\left(K_{1,c}c_1 - C_{1,p}\right) - z_1 c_1\left(\frac{Ac_1 + Bc_2 - EC_{1,p} - GC_{2,p} - HX_d}{Jc_1 + Lc_2 - MX_d}\right) \quad \text{(A4)}$$

Expansion of this expression and collection of the terms gives

$$\frac{dc_1}{dx} = \frac{S_1 c_1^2 + S_2 c_1 c_2 + \left(S_3 X_d + S_4 C_{1,p} + S_5 C_{2,p}\right) c_1 - S_6 C_{1,p} c_2 + S_7 X_d C_{1,p}}{J c_1 + L c_2 - M X_d}, \quad \text{(A5)}$$

where

$$P = \frac{K_{1,c} V}{D_{1,p}}, \qquad Q = \frac{V}{D_{1,p}}, \qquad S_1 = JP - z_1 A,$$

$$S_2 = LP - z_1 B,$$

$$S_3 = z_1 H - MP, \qquad S_4 = z_1 E - JQ, \qquad S_5 = z_1 G,$$

$$S_6 = LQ, \qquad S_7 = MQ. \quad \text{(A6)}$$

There is an equivalent expression for ion 2

$$\frac{dc_2}{dx} = \frac{T_1 c_2^2 + T_2 c_1 c_2 + \left(T_3 X_d + T_4 C_{2,p} + T_5 C_{1,p}\right) c_2 - T_6 C_{2,p} c_1 + T_7 X_d C_{2,p}}{J c_1 + L c_2 - M X_d}, \quad \text{(A7)}$$

where

$$U = \frac{K_{2,c} V}{D_{2,p}}, \qquad Y = \frac{V}{D_{2,p}}, \qquad T_1 = LU - z_2 B,$$

$$T_2 = JU - z_2 A,$$

$$T_3 = z_2 H - MU, \qquad T_4 = z_2 G - LY, \qquad T_5 = z_2 E,$$

$$T_6 = JY, \qquad T_7 = MY \quad \text{(A8)}$$

If these concentration gradients are linearized as before, then

$$\frac{\Delta c_1}{\Delta x} = \frac{S_1 c_{1,\mathrm{av}}^2 + S_2 c_{1,\mathrm{av}} c_{2,\mathrm{av}} + \left(S_3 X_d + S_4 C_{1,p} + S_5 C_{2,p}\right) c_{1,\mathrm{av}} - S_6 C_{1,p} c_{2,\mathrm{av}} + S_7 X_d C_{1,p}}{J c_{1,\mathrm{av}} + L c_{2,\mathrm{av}} - M X_d} \quad \text{(A9)}$$

$$\frac{\Delta c_2}{\Delta x} = \frac{T_1 c_{2,\mathrm{av}}^2 + T_2 c_{1,\mathrm{av}} c_{2,\mathrm{av}} + \left(T_3 X_d + T_4 C_{2,p} + T_5 C_{1,p}\right) c_{2,\mathrm{av}} - T_6 C_{2,p} c_{1,\mathrm{av}} + T_7 X_d C_{2,p}}{J c_{1,\mathrm{av}} + L c_{2,\mathrm{av}} - M X_d} \quad \text{(A10)}$$

It is worth noting that, as opposed to the case of single electrolytes, it is no longer possible to rearrange these expressions to obtain $C_{1,p}$ or $C_{2,p}$ explicitly, which will have a significant effect on the numerical methods used.

The final form of the partitioning expressions at the pore inlet and outlet depends specifically on the valences of the ion present. In the present example, we will study electrolyte mixtures with one univalent anion and cation and a divalent ion, the system of partitioning expressions, and the solution method, which will be shown at the pore inlet (an equivalent expression being obtained at the pore outlet). In order to express $c_2(0)$ and $c_3(0)$ in terms of $c_1(0)$, we will again equate Donnan potentials

$$\Delta\psi_{1,D}(0) = \Delta\psi_{2,D}(0)$$

$$\therefore \frac{1}{z_1} \ln\left(\frac{c_1(0)}{\Phi_1' C_{1,w}}\right) = \frac{1}{z_2} \ln\left(\frac{c_2(0)}{\Phi_2' C_{2,w}}\right) \quad \text{(A11)}$$

$$\Delta\psi_{1,D}(0) = \Delta\psi_{3,D}(0)$$

$$\therefore \frac{1}{z_1} \ln\left(\frac{c_1(0)}{\Phi_1' C_{1,w}}\right) = \frac{1}{z_3} \ln\left(\frac{c_3(0)}{\Phi_3' C_{3,w}}\right) \quad \text{(A12)}$$

Algebraic manipulations of Eqs. A11 and A12 yields

$$c_2(0) = \Phi_2' C_{2,w} \left(\frac{c_1(0)}{\Phi_1' C_{1,w}}\right)^{z_2/z_1}$$

$$c_3(0) = \Phi_3' C_{3,w} \left(\frac{c_1(0)}{\Phi_1' C_{1,w}}\right)^{z_3/z_1} \quad \text{(A13)}$$

Substitution of Eq. A13 into the pore electroneutrality condition and rearrangement gives the following expression (there being an equivalent at the pore outlet)

$$z_1 c_1(0) + z_2 \Phi_2' C_{2,w} \left(\frac{c_1(0)}{\Phi_1' C_{1,w}}\right)^{z_2/z_1} + z_3 \Phi_3' C_{3,w} \left(\frac{c_1(0)}{\Phi_1' C_{1,w}}\right)^{z_3/z_1} + X_d = 0 \quad \text{(A14)}$$

For the electrolyte mixtures studied in this article (Na^+:SO_4^{2-}:Cl^- and Cl^-:Mg^{2+}:Na^+), the ion valences are $+1:-2:-1$ and $-1:+2:+1$, respectively. The ions are ordered in this way because introduction of these valences into Eq. A14 and rearrangement yields the same cubic equations at the pore inlet and outlet

$$z_1 c_1^3(0) + X_d c_1^2(0) + z_3 \Phi'_1 \Phi'_3 C_{1,w} C_{3,w} c_1(0) + z_2 (\Phi'_1)^2 \Phi'_2 C_{1,w}^2 C_{2,w} = 0 \quad \text{(A15)}$$

$$z_1 c_1^3(\Delta x) + X_d c_1^2(\Delta x) + z_3 \Phi'_1 \Phi'_3 C_{1,p} C_{3,p} c_1(\Delta x) + z_2 (\Phi'_1)^2 \Phi'_2 C_{1,p}^2 C_{2,p} = 0 \quad \text{(A16)}$$

Solution of Eqs. A15 and A16 using the Newton–Raphson method shows that there is one real root to each equation, the other two roots being imaginary. If all three ions were univalent, the equivalent of Eqs. A15 and A16 would be quadratic equations, whereas the presence of a trivalent ion would lead to a quartic equation. The overall iterative procedure for three ions is different to that for a single electrolyte, as it is necessary to make guesses for two variables, $C_{1,p}$ and $C_{2,p}$. The method is as follows:

(1) Estimate values of $C_{1,p}$ and $C_{2,p}$.

(2) Calculate $C_{3,p}$ from the permeate electroneutrality condition.

(3) Solve Eqs. A15 and A16 to find $c_1(0)$ and $c_1(\Delta x)$ and calculate $c_2(0)$, $c_3(0)$, $c_2(\Delta x)$, and $c_3(\Delta x)$ from Eq. A13 and the equivalent expressions at the pore outlet.

(4) Calculate $c_{1,\text{av}}$, $c_{2,\text{av}}$, and $c_{3,\text{av}}$ as for single electrolytes.

(5) Substitute all known variables into Eqs. A9 and A10 to calculate Δc_1 and Δc_2. (An arbitrary value of Δx must be included in the calculation, although the value will not affect rejection.) It is possible to calculate $c_i(0)$ and $c_2(0)$ as follows

$$c_i(0) = c_i(\Delta x) - \Delta c_i \quad \text{(A17)}$$

(6) These pore inlet concentrations have now been calculated in two ways, one of which was independent of the iterative guesses of $C_{1,p}$ and $C_{2,p}$. The two test functions will then simply be a comparison of these inlet concentrations

$$f_1 = c_1(0)_{\text{Eq. A15}} - c_1(0)_{\text{Eqs. A9,A10,A17}} = 0$$

$$f_2 = c_2(0)_{\text{Eqs. A13,A15}} - c_2(0)_{\text{Eqs. A9,A10,A17}} = 0 \quad \text{(A18)}$$

A simple way to approach this problem is to combine the test functions and make it always a positive value. The numerical procedure becomes a minimization method in two dimensions, where the minimum equaling zero is the desired root. The easiest way to combine the test functions is as follows:

$$f_T = f_1^2 + f_2^2 = 0 \quad \text{(A19)}$$

In this study, the Star minimization method (Acton, 1970) was used to carry out the iteration. In most studies of multicomponent electrolytes, the modified Powell-hybrid method has been used through the use of numerical algorithm group (NAG) algorithms. The use of such complex numerical methods is limited considerably by the requirement of accurate initial estimates of the permeate concentrations. In contrast, the Star method could be initialized at the low concentration corner of the $C_{1,p} - C_{2,p}$ plane and then moved toward the required solution, because in this case, the overall test function is smooth over the physically realistic range of permeate concentrations, thus removing the dependency on accurate initial estimates.

Manuscript received Apr. 26, 2001, and revision received Oct. 2, 2001.